Available online at www.sciencedirect.com

ScienceDirect

journal homepage: www.elsevier.com/locate/he

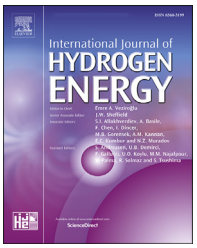

Ru-core Ir-shell electrocatalysts deposited on a surface-modified Ti-based porous transport layer for polymer electrolyte membrane water electrolysis

Masahiro Yasutake [a,b], *Zhiyun Noda* [c], *Junko Matsuda* [b,c,d], *Stephen M. Lyth* [b,c,e], *Masamichi Nishihara* [b], *Kohei Ito* [a,b,c], *Akari Hayashi* [a,b,c,d], *Kazunari Sasaki* [a,b,c,d,*]

[a] *Department of Hydrogen Energy Systems, Faculty of Engineering, Kyushu University, Motooka 744, Nishi-ku, Fukuoka 819-0395, Japan*

[b] *Next-Generation Fuel Cell Research Center (NEXT-FC) Kyushu University, Motooka 744, Nishi-ku, Fukuoka 819-0395, Japan*

[c] *International Research Center for Hydrogen Energy, Kyushu University, Motooka 744, Nishi-ku, Fukuoka 819-0395, Japan*

[d] *Platform of Inter-/ Transdisciplinary Energy Research (Q-PIT), Kyushu University, Motooka 744, Nishi-ku, Fukuoka 819-0395, Japan*

[e] *Department of Chemical and Process Engineering, University of Strathclyde, 75 Montrose St, Glasgow G1 1XL, United Kingdom*

HIGHLIGHTS

- Ru-core Ir-shell electrocatalysts were prepared on Ti-based porous transport layers.
- The activation overvoltage was significantly lower compared to pure Ir electrocatalysts.
- The durability of the electrocatalyst was improved by increasing the Ir-to-Ru ratio.
- This unique electrode can operate at high current densities up to 10 A cm^{-2}.

ARTICLE INFO

Article history:
Received 13 May 2023
Received in revised form
5 July 2023
Accepted 6 July 2023
Available online xxx

Keywords:
Polymer electrolyte membrane water electrolysis
Core-shell catalyst

ABSTRACT

Novel Ru-core Ir-shell catalyst-integrated porous transport electrodes (PTEs) for polymer electrolyte membrane water electrolysis (PEMWE) cells are prepared, in which Ru-core Ir-shell catalyst nanostructures are directly deposited onto a porous transport layer (PTL) via arc plasma deposition (APD). The PTL has a nanostructured TiO_2 surface prepared via NaOH etching, acting as a catalyst support. The performance and durability of these Ru-core Ir-shell catalysts depend strongly on the ratio of Ir and Ru. The current-voltage (I–V) characteristics of PEMWE cells were improved by applying these core-shell catalysts with a low Ir loading of around 0.1 mg cm^{-2}. The core-shell catalyst-integrated PTEs can operate at current densities of up to 10 A cm^{-2} without exhibiting limiting current behavior. This unique combination of the core-shell catalyst and the PTE structure enables

* *Corresponding author*. Department of Hydrogen Energy Systems, Faculty of Engineering, Kyushu University, Motooka 744, Nishi-ku, Fukuoka 819-0395, Japan.
E-mail address: sasaki@mech.kyushu-u.ac.jp (K. Sasaki).

https://doi.org/10.1016/j.ijhydene.2023.07.048

Porous transport electrode
High current density operation
Low iridium loading

PEMWE cell operation with low iridium loading and high current density, potentially reducing the cost of green hydrogen.

Introduction

The Intergovernmental Panel on Climate Change (IPCC) has strongly requested continuous actions in response to the climate crisis [1]. The necessity of reducing greenhouse gas emissions caused by human activities and realizing carbon neutrality is clear for the mitigation of climate change. There are several strategies towards carbon neutrality, including improvement in energy efficiency, increasing the fraction of renewable energy, a transition from fossil fuels to alternative decarbonized fuels such as hydrogen, and the introduction of carbon capture, storage, and utilization technologies [2]. Regarding renewable energy, chemical energy carriers are necessary due to the fluctuation in power generation of solar and wind power, depending on the weather conditions or time of day. Hydrogen is a prospective candidate as an energy carrier for renewable energy storage and transportation [3,4]. Green hydrogen, which is defined as originating from renewable energy sources, can be produced via the electrolysis of water.

Polymer electrolyte membrane water electrolysis (PEMWE) can operate at relatively low temperature and high current densities with quick load response, enabling compact and robust electrolysis systems. However, the higher capital expenditure (CAPEX) of PEMWEs prevents widespread commercialization compared to alternatives such as alkaline water electrolysis systems. One of the origins of such high CAPEX is the use of platinum group metal (PGM) catalysts such as iridium and platinum.

Other components in PEMWE cells besides the catalysts are also relatively expensive, such as the polymer electrolyte membranes, the platinum-coated titanium-based PTLs, and the separators. Operation at a high current density can reduce the cost of green hydrogen by decreasing the overall required electrode area, materials cost, and thus the CAPEX. Meanwhile, alkaline water electrolysis is widely used for commercial hydrogen production, but has material-related limitations due to, *e.g.*, high ohmic resistance, under high current density operation. In contrast, PEMWEs can be operated at higher current densities, which is advantageous compared to other types of water electrolysis technologies. In demonstration of this, Villagra et al. studied the relationship between CAPEX and operating expense (OPEX) in PEMWE cells at high current densities. They found an optimal operating current density of 2–3 A cm^{-2} at < 2 V (the voltage selected to prevent IrO_2 dissolution). If cell performance can be improved, a higher optimum value of around 10 A cm^{-2} may be expected [5]. Therefore, lower PGM loading and overall electrode area reduction by increasing current density are essential for the reduction of CAPEX in PEMWEs.

Decreasing the anode catalyst loading is particularly critical for CAPEX reduction, because a large amount of PGM catalysts with iridium loading around 5 mg cm^{-2} is often used for the rate-determining anodic reaction. A significant reduction in PGM catalyst loading to <0.2 mg cm^{-2} is required in the future, according to an International Renewable Energy Agency report [6]. Ru-based and Ir-based catalysts have been applied as anode catalysts by many researchers [7–16]. Ru has the highest oxygen evolution reaction (OER) activity [17] but a low stability in the strongly acidic and high-potential PEMWE environment. Therefore, Ir-based catalysts, which have a lower OER activity but higher stability compared to Ru-based catalysts, are generally used in commercial PEMWE cells.

However, applying highly active and inexpensive Ru-based catalysts may be attractive for highly efficient and low-cost water electrolysis systems [18–20]. Researchers have studied to improve the stability of Ru-based catalysts by alloying, mixing with oxides, and structural control [21–23]. For example, Wu et al. developed Ru–Ir catalysts with a unique coral-like structure consisting of 3-nm-thick sheets. The Ru–Ir catalysts exhibited higher OER activity and remained stable for 120 h at 1.485 V, compared with the single-element catalysts of Ir and Ru [24]. Besides tailoring composites and alloying, Ru catalysts coated with protective Ir, *i.e.*, employing a core-shell structure, have been developed to improve catalytic activity and stability [25]. Seow et al. [26] and Shan et al. [27] both prepared Ru–Ir core-shell catalysts, and their core-shell catalysts exhibited higher OER activity and durability compared to Ir-based, Ru-based, and Ir–Ru alloy catalysts. However, all of these evaluations were performed in half-cell tests, and the stability of these catalyst systems under practical operating conditions between 1.5 V and 2.0 V at the single cell level has not yet been demonstrated to the best of our knowledge.

In addition to optimizing the catalyst structure, optimization of the porous transport electrode (PTE) structure can also improve catalyst utilization and simplify the manufacturing process [28,29]. For example, Kim et al. deposited Ir catalyst on a dendritic gold structure on a carbon-based PTL, resulting in high electrolysis performance with low Ir loading of 10 μg cm^{-2} [30]. Similarly, Laube et al. developed PTEs with high electrolysis performance, where Ir catalyst was deposited on a Ti-based PTL via atomic layer deposition [31]. Our research group has previously developed PTEs, where Ir catalysts were deposited on Ti oxide nanotubes on Ti-based PTLs [32–36]. Such PTE exhibited relatively high electrolysis performance, despite low Ir loading of around 0.2 mg cm^{-2}. Depositing binary catalysts such as alloys or core-shell structures on this PTE structure is a promising strategy for further reducing iridium loading and increased catalytic activity.

Please cite this article as: Yasutake M et al., Ru-core Ir-shell electrocatalysts deposited on a surface-modified Ti-based porous transport layer for polymer electrolyte membrane water electrolysis, International Journal of Hydrogen Energy, https://doi.org/10.1016/j.ijhydene.2023.07.048

Here, we investigate Ru-core Ir-shell electrocatalysts on the surface-modified Ti-based PTLs, as schematically shown in Fig. 1. The performance and durability of such electrocatalysts are evaluated under practical operation conditions with a single cell setup. Ru-core Ir-shell electrocatalysts are deposited on the PTLs via APD, which is a type of physical vapor deposition. The surface-modified PTLs are prepared by NaOH treatment forming titanium oxide nanofibers, increasing specific surface area, and acting as catalyst supports [32–34]. Our previous study determined the optimal NaOH treatment conditions to increase specific surface area and catalytic activity. Moreover, PGM catalyst layers in this structure can eliminate the need for platinum coatings on the PTL. In PTEs, the electrocatalysts act as an electron-conductive coating, and the PTL itself acts as the catalyst support. Electrodes designed in this way therefore do not have a thick catalyst layer made by conventional noble-metal powder catalysts, enabling high current density operation by suppressing the mass transport overvoltage.

In this study, the I–V characteristics beyond 12 A cm^{-2} are measured, the performance and durability of Ru-core Ir-shell catalyst-integrated PTEs are evaluated, and remaining technological issues are clarified.

Experimental and calculation procedure

Preparation of Ru-core Ir-shell catalyst-integrated PTEs

The procedure for preparing the PTEs is summarized in Fig. 2. Titanium microfiber sheets with nominal porosity of 70% (Nikko Techno, Ltd., Osaka, Japan) were used as starting materials for the PTLs. Meanwhile, the average porosity of the samples calculated from their thickness and weight was 75.1 ± 2%. The discrepancy between these two values may arise from, *e.g.*, the surface roughness of such porous materials, affecting their thickness as measured by a micrometer. The titanium microfiber sheets are *ca.* 200 μm thick, which are made of interconnecting titanium microfibers with individual cross sections of approximately 10 μm by 10 μm.

In order to increase the surface area of the titanium PTLs, chemical etching with NaOH solution was performed [30]. First, titanium sheets were etched in an aqueous 1 M NaOH solution (Kishida Chemical Co., Ltd., Osaka, Japan) at 60 °C for 1 h. After that, the etched titanium sheets were washed under ultra-sonication in 0.01 M HNO_3 solution (Kishida Chemical Co., Ltd., Osaka, Japan) for 30 min and then washed in deionized water at room temperature for 10 min for complete neutralization. The samples were then heat treated at 400 °C in 5% H_2–N_2 gas (50 ml min^{-1}) for 30 min, with a heating rate of 5 °C min^{-1}. Results reporting the optimization of NaOH etching conditions have been published elsewhere [36].

Iridium and ruthenium were deposited onto the NaOH-etched titanium sheets at room temperature via arc plasma deposition (APD-S, Advanced RIKO, Inc., Yokohama, Japan) [37], in a vacuum at a pressure of 10^{-3} Pa; a discharge voltage of −100 V; a capacitance of 1080 μF; and a discharge frequency of 3 Hz. Iridium and ruthenium loading was controlled by varying the number of APD pulses [36]. The Ru-core Ir-shell catalyst structure was prepared by Ru deposition followed by Ir deposition.

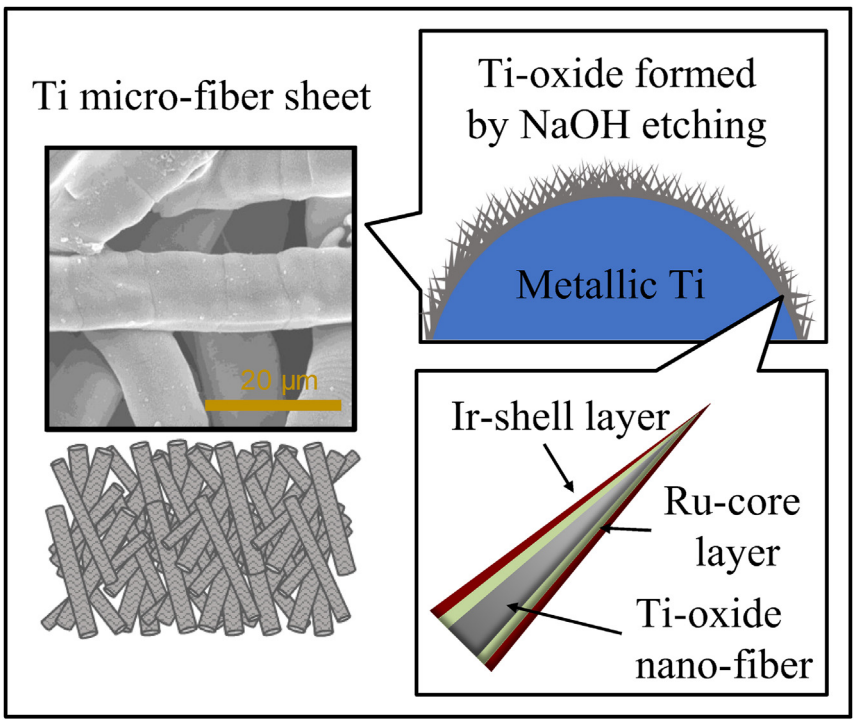

Fig. 1 – Schematic diagrams showing the concept of the core-shell catalyst-integrated porous transport electrode (PTE) with a titanium porous transport layer (PTL), nanostructured titanium oxide as a catalyst support, and a Ru-core Ir-shell layer acting as an electrocatalyst.

Please cite this article as: Yasutake M et al., Ru-core Ir-shell electrocatalysts deposited on a surface-modified Ti-based porous transport layer for polymer electrolyte membrane water electrolysis, International Journal of Hydrogen Energy, https://doi.org/10.1016/j.ijhydene.2023.07.048

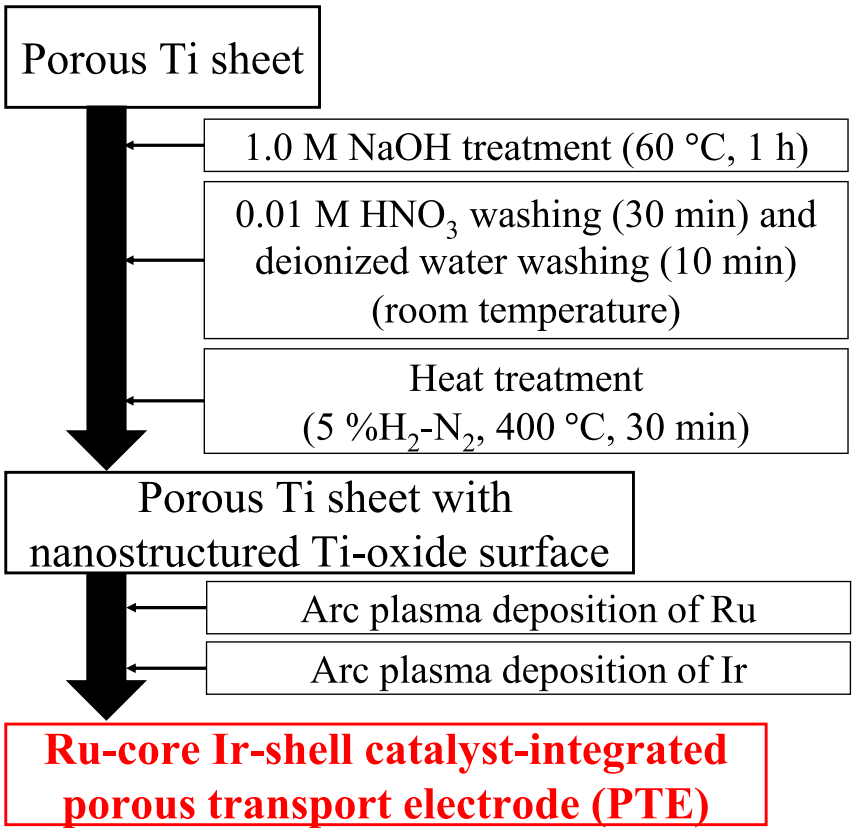

Fig. 2 – Preparation procedure for the Ru-core Ir-shell catalyst-integrated porous transport electrode (PTE).

Characterization of electrodes

The microstructure of the electrodes was observed by scanning transmission electron microscopy (STEM, JEM-ARM200F, JEOL Ltd., Tokyo, Japan) in combination with energy dispersive X-ray spectroscopy (EDS). The acceleration voltage was 200 kV. The crystal structures of iridium and ruthenium related materials were identified by analyzing their selected-area electron diffraction patterns (SAEDPs).

Ir and Ru loadings deposited on the Ti sheets by APD were derived using a calibration curve. This calibration curve was prepared by measuring Ir loading per unit area on carbon paper instead of Ti sheets, using thermogravimetry in air (Thermo Plus TG8121, Rigaku Co., Tokyo, Japan) [36]. First, iridium and ruthenium were deposited onto carbon papers via APD with various numbers of pulses, and then the Ir and Ru loadings per unit area and unit number of pulses were obtained by measuring the weight of iridium remaining after oxidative removal of the carbon papers during TG measurements. The measured Ir and Ru loading per 1000 APD pulses were 0.043 $mg_{\cdot Ir}$ cm^{-2} and 0.039 $mg_{\cdot Ru}$ cm^{-2}, respectively.

Thermochemical equilibrium calculation

Pourbaix diagrams for evaluating the stability of materials at a given pH and potential were calculated using HSC Chemistry ver.9.0 software (Outotec Research Oy., Pori, Finland). Ir–H_2O and Ru–H_2O materials systems are derived and analyzed.

Preparation of membrane electrode assemblies (MEAs)

MEAs were prepared with an electrode size of 1.0 cm^2 (1 cm by 1 cm) and a Pt loading of 0.5 $mg_{\cdot Pt}$ cm^{-2} for the PEMWE cathode. To evaluate the effect of the Ir/Ru loading ratio on the cell

Table 1 – Specifications of the various Ir/Ru/Ti electrodes.

Samples (Element - APD pulses)	Iridium loading/mg cm^{-2}	Ruthenium loading/mg cm^{-2}	Total PGM loading/mg cm^{-2}
Ir-4000	0.172	(none)	0.172
Ir-3000	0.129	(none)	0.129
Ir-3000/Ru-1000	0.129	0.039	0.168
Ir-2000/Ru-2000	0.086	0.078	0.164
Ir-1000/Ru-3000	0.043	0.117	0.160
Ru-4000	(none)	0.156	0.156

Please cite this article as: Yasutake M et al., Ru-core Ir-shell electrocatalysts deposited on a surface-modified Ti-based porous transport layer for polymer electrolyte membrane water electrolysis, International Journal of Hydrogen Energy, https://doi.org/10.1016/j.ijhydene.2023.07.048

performance, the Ir and Ru loadings on the anode were adjusted as compiled in Table 1.

An electrocatalyst paste for the PEMWE cathodes was prepared by dispersing Pt/C (Pt 46.5%, TEC10E50 E, Tanaka Kikinzoku Kogyo Co., Tokyo, Japan), 99.5% ethanol, deionized water, and 5% Nafion solution using an ultrasonic homogenizer. The Nafion ratio (the weight ratio of Nafion in the total weight of Nafion and the Pt/C catalyst) in the cathode electrocatalyst layer was set to be 28 wt%. This electrocatalyst paste was printed onto the electrolyte membrane (Nafion117, E. I. du Pont de Nemours and Co., Wilmington, USA) using a spray printing system (C-3 J, Nordson Co., Westlake, USA).

The PTEs decorated with the Ru-core Ir-shell catalysts were applied as PEMWE anodes. MEAs were prepared by hot-pressing the PTEs with the cathode catalyst-coated electrolyte membranes at 140 °C and 0.3 MPa for 180 s. Carbon paper (EC-TP1-060T, ElectroChem Inc., Raynham MA, USA) was used as the PTL on the cathode side. No additional PTL was used at the anode, since the catalyst-integrated PTE acts as an integrated PTL. The tightening torque was typically set to 4 N m for assembling an MEA in a PEMWE cell holder.

Characterization of MEAs

The I–V characteristics of the electrolysis cells were evaluated at 80 °C by supplying deionized water (5 ml min^{-1}) using a commercial cell holder (Eiwa Co., Osaka, Japan). Before the electrochemical measurements, deionized water was supplied for 2 days to sufficiently hydrate the polymer electrolyte membrane. I–V curves were obtained by measuring the current density with increasing cell voltage applied from 1.3 V to 2.0 V using an electrochemical analyzer (SI 1287, AMETEK Inc., Berwyn, USA). I–V curves in the high current density range up to *ca.* 12 A cm^{-2} were analyzed with increasing cell voltage from 1.3 V to 3.5 V using a bipolar power supply (PBZ20-20A, Kikusui Electronics Corp., Yokohama, Japan) and a data logger (midi LOGGER HV GL2000, Graphtec Corp., Yokohama, Japan).

An alternative current (AC) impedance analyzer (1255B, AMETEK Inc., Berwyn, USA) was used to extract the ohmic resistance. The activation overvoltage and concentration overvoltage were then separated along with the procedure used for PEFC evaluations as follows [38]. A Tafel plot was first created with current density on a logarithmic x-axis and the IR-free cell voltage on the y-axis. In the low current density region, 6 values were fitted with linear regression. The difference between the theoretical electromotive force (1.17 V at 80 °C, at ambient pressure) and the voltage of the linear regression line was taken as the activation overvoltage at the current density of interest. The deviation of IR-free voltage from the voltage in the linear regression line in the Tafel plot was taken as the mass transport overvoltage [38].

The electrode durability of single cells was evaluated at constant potential of 1.6 V for 100 h, whilst I–V curves and impedance spectra were recorded before and after durability tests.

All these electrochemical measurements were performed twice or more to check their reproducibility. Representative data is shown in figures. The average and standard deviation of overvoltages are derived and further analyzed.

Results and discussion

Deposition of Ru-core Ir-shell catalyst via APD

Ru-core Ir-shell electrocatalysts were deposited on the titanium oxide nanofibers generated via NaOH etching [30]. Ru-core layer deposition followed by Ir-shell deposition via APD created a core-shell structure on the titanium oxide nanofibers grown on the titanium-fiber-based PTL.

Fig. 3a and b shows a STEM image and a corresponding EDS elemental intensity map of the electrocatalysts consisting of the Ru-core formed via 3000 APD pulses (Ru loading: 0.117 mg cm^{-2}) and the Ir-shell formed via 1000 APD pulses (Ir loading: 0.043 mg cm^{-2}). Red, green, and blue dots indicate Ir, Ru, and Ti in elemental EDS maps of Fig. 3. The number after Ru and Ir in the sample names represents the number of APD pulses, denoted here as Ir-1000/Ru-3000/Ti. Fig. 3a and b confirm that the Ir-1000/Ru-3000/Ti has a Ru-core layer deposited on the NaOH-etched titanium oxide nanofiber of 5–10 nm in diameter, and the Ir layer deposited on the Ru layer. The core-shell structure is clearly observed in Fig. 3b, in which the distributions of Ir, Ru, and Ti are shown. The diameter of the Ru-core-coated fibrous structure is *ca.* 30–50 nm. The thickness of the Ir-shell layer on the Ru-core layer is *ca.* 3–4 nm.

Fig. 3c to f shows (c,e) STEM images and (d,f) corresponding EDS elemental intensity maps of Ir, Ru, and Ti for (c,d) the Ir-2000/Ru-2000/Ti electrode and (e,f) the Ir-3000/Ru-1000/Ti electrode. Increasing Ir/Ru ratio increases the thickness of the Ir-shell layer. The Ir-2000/Ru-2000/Ti and Ir-3000/Ru-1000/Ti electrodes have Ir-shell layers with a thickness of *ca.* 4–6 nm (Fig. 3c and d), and *ca.* 7–10 nm (Fig. 3e and f), respectively. Therefore, varying the number of APD pulses in Ir and Ru deposition can control Ir-shell layer thickness.

Fig. 4 shows a selected area electron diffraction pattern (SAEDP) of the Ir-1000/Ru-3000/Ti electrode. SAEDP analysis can identify the material's crystalline structure in the local area within a few hundred nanometers: the spacing of crystal lattice planes (d) is calculated from the equation of $d = L\lambda/R$, where L is camera length in the microscope, λ wave length of electron beam depending on accelerating voltage (200 kV), and R a distance between the center spot and the diffraction spot in the electron diffract pattern. In Fig. 4, the different radii of diffraction spot rings are attributed to the lattice spacings of Ir and Ru metal crystals. This indicates that the electrocatalyst has a true core-shell structure, rather than forming an alloy, with metallic Ir as a protective layer covering metallic Ru on the titanium oxide nanofiber support.

Thus, this section demonstrated that a core-shell structure consisting of two elements, Ru and Ir, can be fabricated using the APD method on titanium oxide nanofibers on PTLs and that the APD conditions can control such nanostructure. This shows the possibility of fabricating similar nanostructures from other elemental species. It should be noted however that APD is a relatively expensive process for mass production, despite being suitable for fabricating such interesting structures. Fabricating a similars structures by applying more inexpensive procedures such as magnetron sputtering [39,40] is therefore an essential task of future studies.

Please cite this article as: Yasutake M et al., Ru-core Ir-shell electrocatalysts deposited on a surface-modified Ti-based porous transport layer for polymer electrolyte membrane water electrolysis, International Journal of Hydrogen Energy, https://doi.org/10.1016/j.ijhydene.2023.07.048

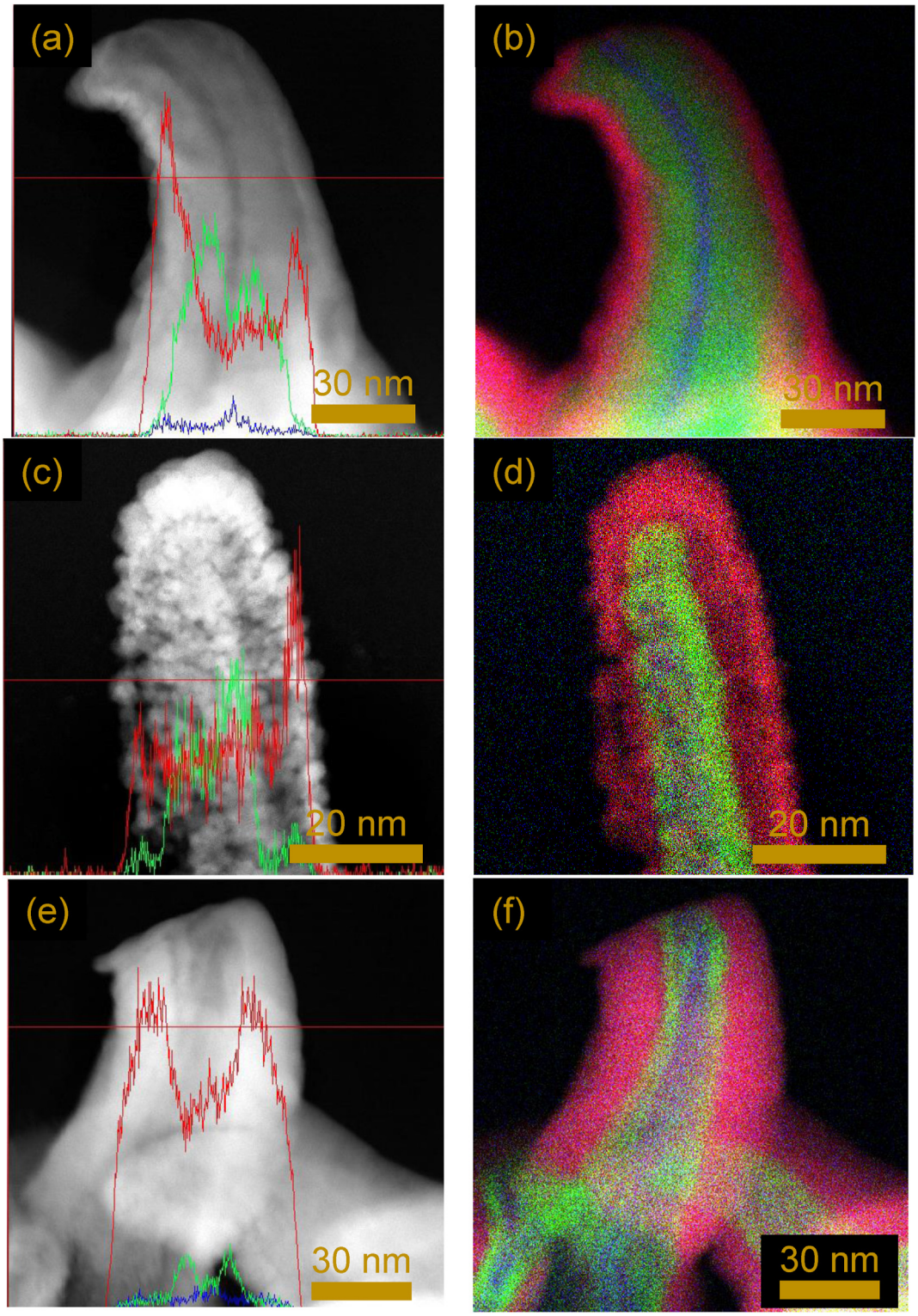

Fig. 3 – STEM images with line analysis data and the corresponding elemental EDS maps of composited Ir, Ru, and Ti for (a, b) the Ir-1000/Ru-3000/Ti, (c,d) the Ir-2000/Ru-2000/Ti, and (e, f) Ir-3000/Ru-1000/Ti electrodes before the durability test. Red, green, and blue dots indicate Ir, Ru, and Ti, respectively in elemental EDS maps.

Electrochemical performance: effect of Ir/Ru ratio

To evaluate the effect of Ir/Ru ratio on cell performance, electrodes were fabricated with various Ir/Ru loading ratios, as compiled in Table 1, and their electrode performance was evaluated. Fig. 5 shows the corresponding (a) I–V characteristics, the comparison of (b) ohmic overvoltage at 1000 mA cm^{-2}, and (c) activation overvoltages at 200 mA cm^{-2}.

Please cite this article as: Yasutake M et al., Ru-core Ir-shell electrocatalysts deposited on a surface-modified Ti-based porous transport layer for polymer electrolyte membrane water electrolysis, International Journal of Hydrogen Energy, https://doi.org/10.1016/j.ijhydene.2023.07.048

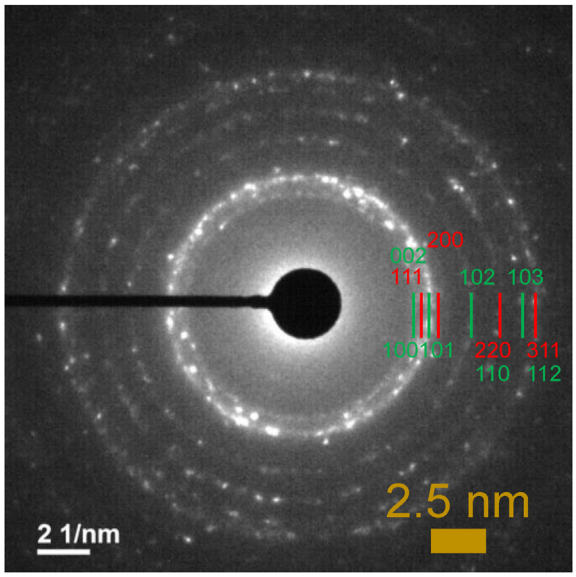

Fig. 4 – SAEDP (selected-area electron diffraction pattern) of the Ru-core Ir-shell catalyst (Ir-1000/Ru-3000/Ti electrode). Each diffraction spot rings is attributed to the lattice spacing of Ir or Ru metal crystal. The red and green indices of lattice planes show those of Ir and Ru crystals, respectively. (Ir has a face-centered cubic structure with a lattice constant *an* of 0.384 nm; Ru a hexagonal structure with *a* and *c* of 0.270 nm and 0.427 nm, respectively.)

Fig. 5 shows the results of the first (initial) and second measurements because the I–V characteristics could differ, as discussed below.

First, the electrochemical performance of the Ru-4000/Ti electrode was analyzed (0.156 mg cm^{-2} Ru). In the I–V characteristics (Fig. 5a), the current density starts to decrease sharply at around 1.55 V as the cell potential (voltage) increases. The decrease in current density during the I–V measurement indicates a rapid degradation in electrode performance because this measurement applied increasing potential scanning. Moreover, the current density could not be increased after the first I–V measurement. This suggests that irreversible degradation (such as detachment and dissolution of Ru) may have occurred. Fig. 6a shows a Pourbaix diagram of the Ru–H_2O system at 80 °C, calculated. The equilibrium potential of Ru/RuO_2 is observed to be *ca.* 0.5 V at pHs ranging from 0 to 1.0 (which corresponds approximately to the pH of strongly-acidic Nafion), and above this value, oxidation of metallic Ru to RuO_2 is expected to occur in the Ru/Ti electrode. Meanwhile, from this Pourbaix diagram, Ru dissolution is expected to occur above *ca.* 1.4 V at such pHs. Therefore, Ru dissolution when scanning from 1.3 V to 2.0 V can be expected to result in the atypical I–V characteristics. Similarly, Reier et al. also reported a decrease in current density above 1.5 V due to Ru dissolution in the rotating disk electrode measurements [41]. The electrolysis voltage at 200 mA cm^{-2} (before Ru dissolution occurs) is 1.45 V for the Ru-4000/Ti, and 1.51 V for the Ir-4000/Ti, as shown in Fig. 5a. These results are consistent because Ru has higher OER activity than Ir [17].

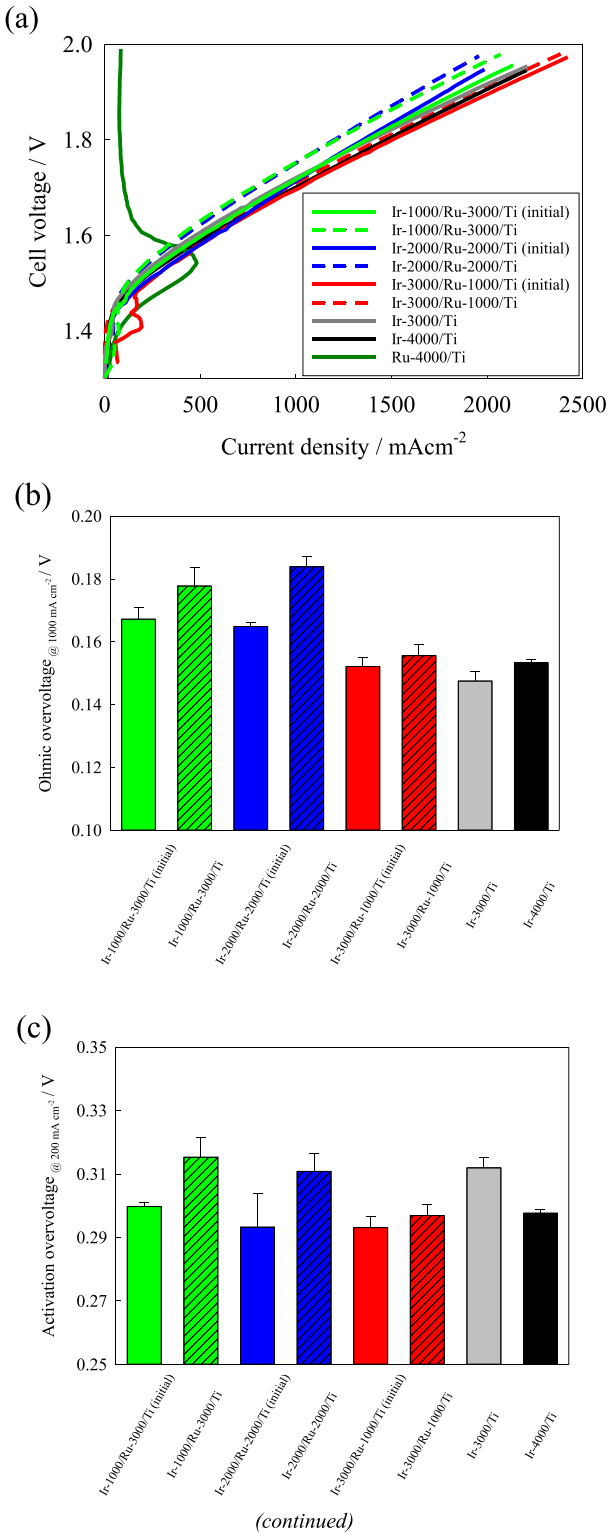

Fig. 5 – (a) I–V characteristics of PEMWE cells using Ir/Ru/Ti electrodes prepared via APD with different ratios of iridium and ruthenium: Comparison of (a) ohmic overvoltage at 1000 mA cm^{-2} and (b) activation overvoltage at 200 mA cm^{-2} of the Ru-core Ir-shell electrodes. The number of APD pulses was varied from 1000 to 4000. The results of both the first (initial) and second measurements are shown.

Please cite this article as: Yasutake M et al., Ru-core Ir-shell electrocatalysts deposited on a surface-modified Ti-based porous transport layer for polymer electrolyte membrane water electrolysis, International Journal of Hydrogen Energy, https://doi.org/10.1016/j.ijhydene.2023.07.048

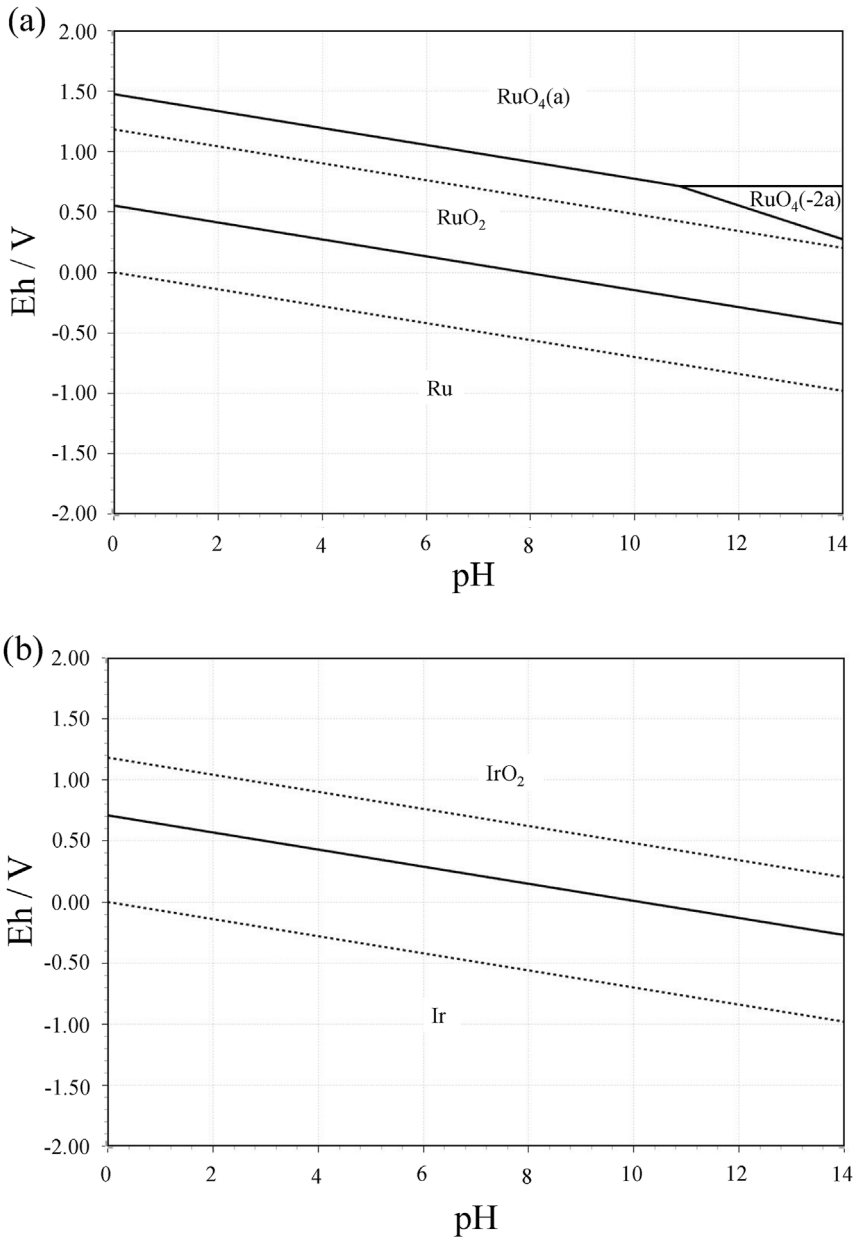

Fig. 6 – Pourbaix diagrams of (a) Ru–H_2O and (b) Ir–H_2O systems at 80 °C, as a function of pH.

Second, the effect of potential scanning during I–V measurements on the I–V characteristics of the Ru-core Ir-shell electrode was investigated. Degradation in the I–V performance of the Ru-core Ir-shell electrode was observed between the first (initial) and second I–V measurements in Fig. 5a. Meanwhile, Fig. 6b shows the Porbaix diagram of the Ir–H_2O system at 80 °C, showing that Ir is stable as an oxide (IrO_2) up to 2.0 V. Therefore, Ir dissolution is unlikely to occur during this I–V measurement between 1.3 V and 2.0 V. This performance degradation is attributed to the dissolution of exposed Ru (which readily dissolves in the measured voltage range, as mentioned above), in areas not sufficiently covered with Ir. The increase in ohmic and activation overvoltages are predominant factors in the I–V performance degradation, as shown in Fig. 5b and c. Our previous study found that coated metallic layers deposited on the PTL via APD not only act as a catalyst but also improve the electronic conductivity, and thus reduce ohmic resistance [36]. Therefore, Ru dissolution and detachment from the Ru-core Ir-shell electrode (which acts as both a catalyst and a conductive coating in the PTL) lead to an increase in both ohmic and activation overvoltages after the first I–V measurement.

Third, the effect of Ir/Ru loading ratio on cell performance was evaluated. Fig. 5 shows (b) ohmic overvoltage at 1000 mA cm^{-2} and (c) activation overvoltage at 200 mA cm^{-2} of the Ru-core Ir-shell electrodes before and after the I–V measurements. The Ir-1000/Ru-3000/Ti electrode and the Ir-2000/Ru-2000/Ti electrode exhibit a significant increase in

Please cite this article as: Yasutake M et al., Ru-core Ir-shell electrocatalysts deposited on a surface-modified Ti-based porous transport layer for polymer electrolyte membrane water electrolysis, International Journal of Hydrogen Energy, https://doi.org/10.1016/j.ijhydene.2023.07.048

ohmic and activation overvoltages after the first I–V measurement, compared to the Ir-3000/Ru-1000/Ti, Ir-3000/Ti, and Ir-4000/Ti electrodes, resulting in lower I–V performance during the second potential cycle. This may be because the ratio of Ir to Ru was lower than that of other electrodes, so that a larger fraction of the Ru layer was not protected by the Ir-shell, causing more significant Ru dissolution and thus cell degradation. In fact, lower Ir-to-Ru (Ir/Ru) ratio caused an increase in ohmic and activation overvoltages. Fig. 7 shows (a) a STEM image and (b-e) corresponding EDS elemental intensity maps of the Ir-1000/Ru-3000/Ti electrode after the I–V measurement. The Ru-core Ir-shell structure was maintained.

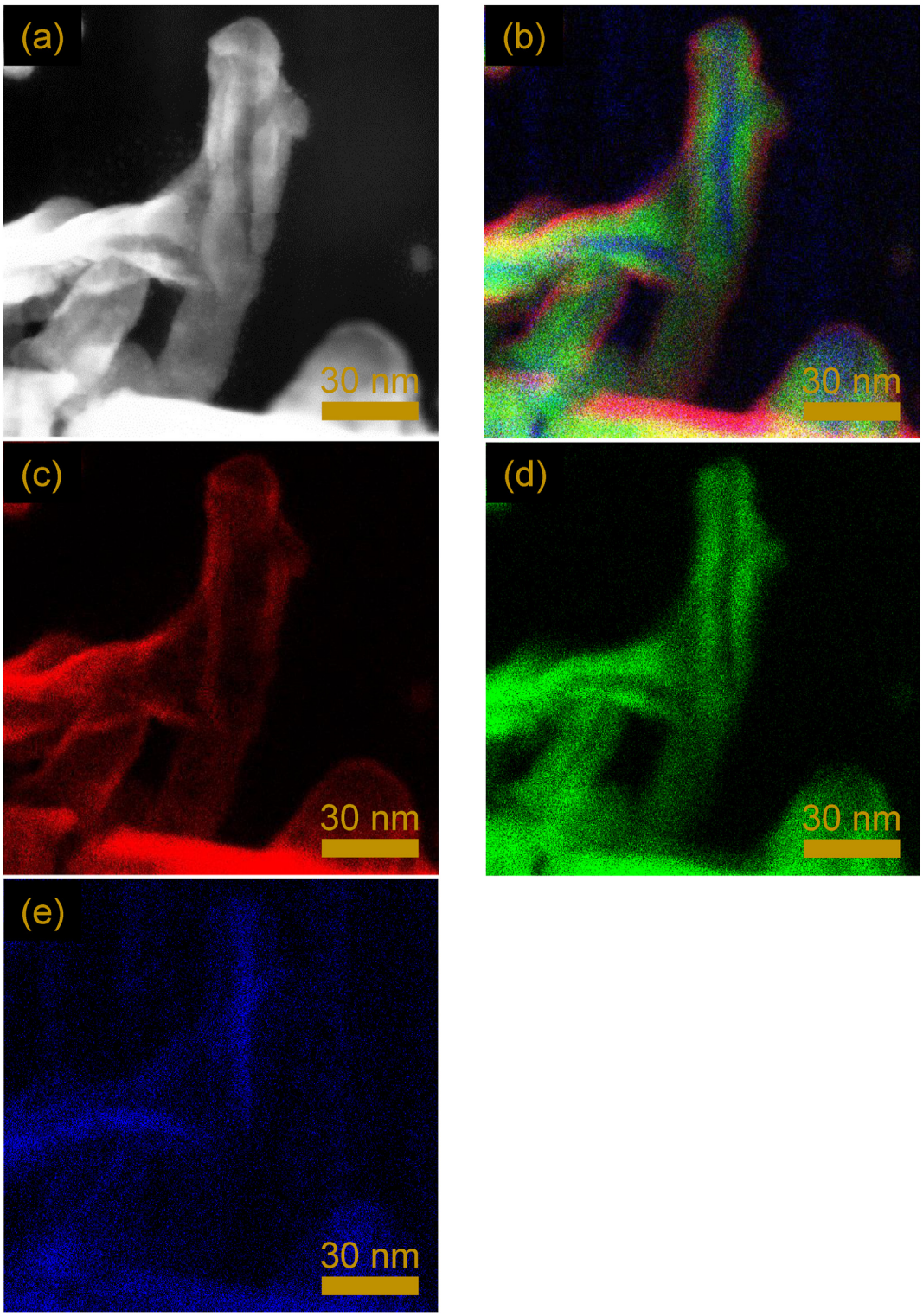

Fig. 7 – (a) STEM image, and corresponding EDS elemental maps of (b) Ir + Ru + Ti, (c) Ir (red), (d) Ru (green), and (e) Ti (blue), for the Ir-1000/Ru-3000/Ti porous transport electrode after the I–V measurement.

Please cite this article as: Yasutake M et al., Ru-core Ir-shell electrocatalysts deposited on a surface-modified Ti-based porous transport layer for polymer electrolyte membrane water electrolysis, International Journal of Hydrogen Energy, https://doi.org/10.1016/j.ijhydene.2023.07.048

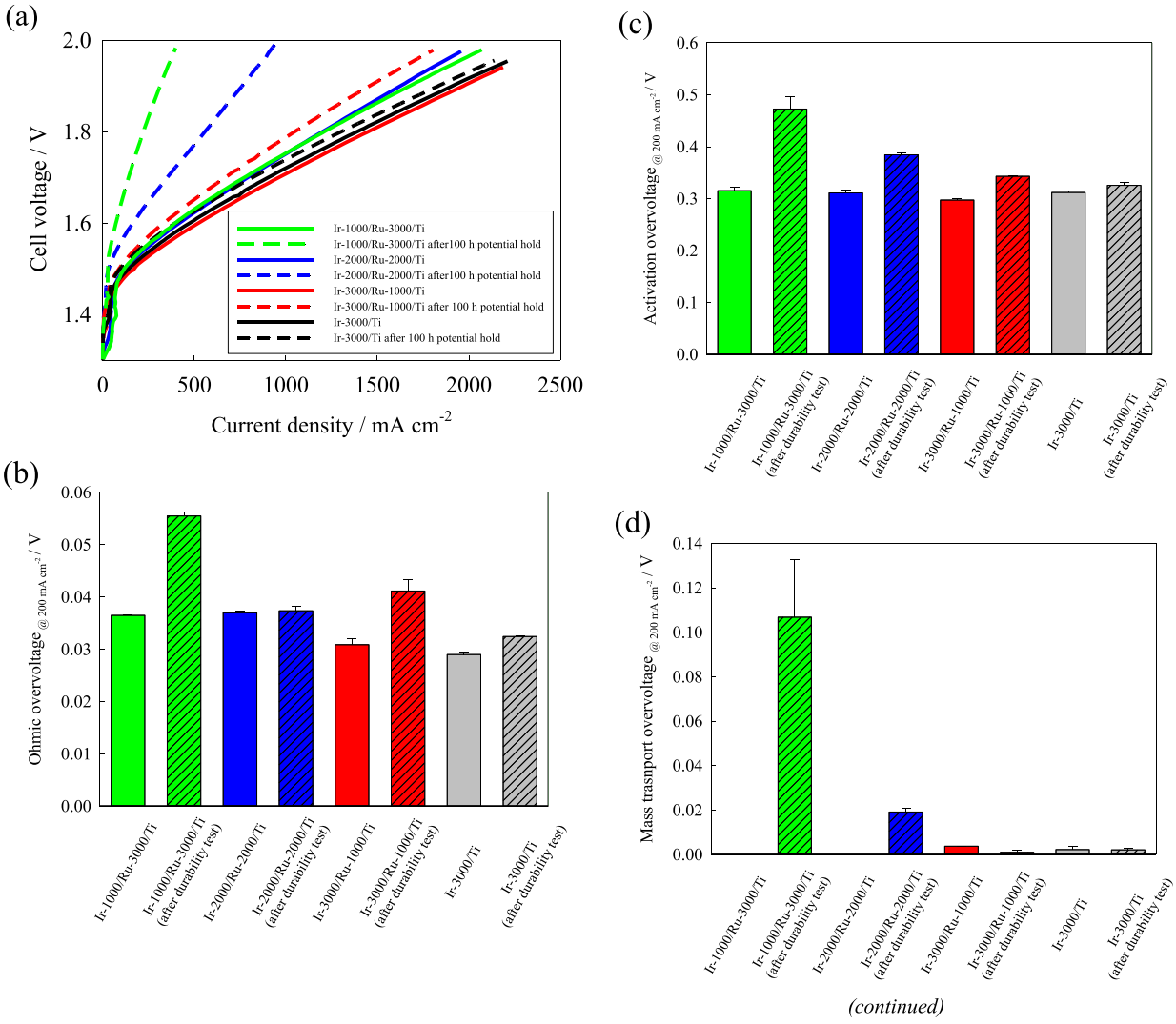

(continued)

Fig. 8 – Electrochemical properties of PEMWE cells using various Ru-core Ir-shell electrodes prepared via APD with different ratios of iridium and ruthenium before and after a 100-h constant voltage durability test at 1.6 V: (a) I–V characteristics; the comparison of (b) ohmic, (c) activation, and (d) mass transport overvoltage at 200 mA cm^{-2}. The results using Ir-3000/Ti electrode are also shown.

However, the atomic Ir/Ru ratio detected by EDS after the I–V measurement was 0.45, indicating an increase in the Ir/Ru ratio, compared to 0.28 before the I–V measurement. This indicates that the Ir/Ru ratio increased due to the dissolution of Ru uncoated by Ir during the I–V measurement. These results indicate that the Ir-shell acts as a protective layer for Ru, but also that a sufficiently thick Ir-shell is needed to prevent Ru dissolution.

The number of active sites on the catalyst surface could depend on the Ir loading since Ru without Ir protection dissolved even after the first I–V measurement. Therefore, the number of active sites for the Ir-3000/Ti and Ir-3000/Ru-1000/Ti electrodes may be similar due to the same Ir loading. Fig. 5c compares the activation overvoltage of the Ir-3000/Ti, Ir-4000/Ti, and Ir-3000/Ru-1000/Ti electrodes at 200 mA cm^{-2}. The Ir-3000/Ru-1000/Ti electrode exhibited lower activation overvoltage than the Ir-3000/Ti electrode, but comparable to the Ir-4000/Ti electrode. Therefore, the lower activation overvoltage of the Ir-3000/Ru-1000/Ti electrode compared to the Ir-3000/Ti electrode can be attributed to the improved specific activity due to the core-shell structure.

This section confirmed that the Ru-core Ir-shell structure can partly prevent Ru dissolution, while Ru easily dissolved during potential scanning. The core-shell structure may also reduce the initial activation overvoltage. Ir-3000/Ru-1000/Ti (Ir loading: 0.129 mg cm^{-2}) exhibited the equivalent initial performance compared with Ir-4000/Ti (Ir: loading: 0.172 mg cm^{-2}); thus, this catalyst structure also contributes to reducing the Ir loading in PEM electrolyzers.

Durability: effect of Ir/Ru ratio

Fig. 8 shows (a) I–V characteristics and the comparison of (b) ohmic, (c) activation, and (d) mass transport overvoltages at

Please cite this article as: Yasutake M et al., Ru-core Ir-shell electrocatalysts deposited on a surface-modified Ti-based porous transport layer for polymer electrolyte membrane water electrolysis, International Journal of Hydrogen Energy, https://doi.org/10.1016/j.ijhydene.2023.07.048

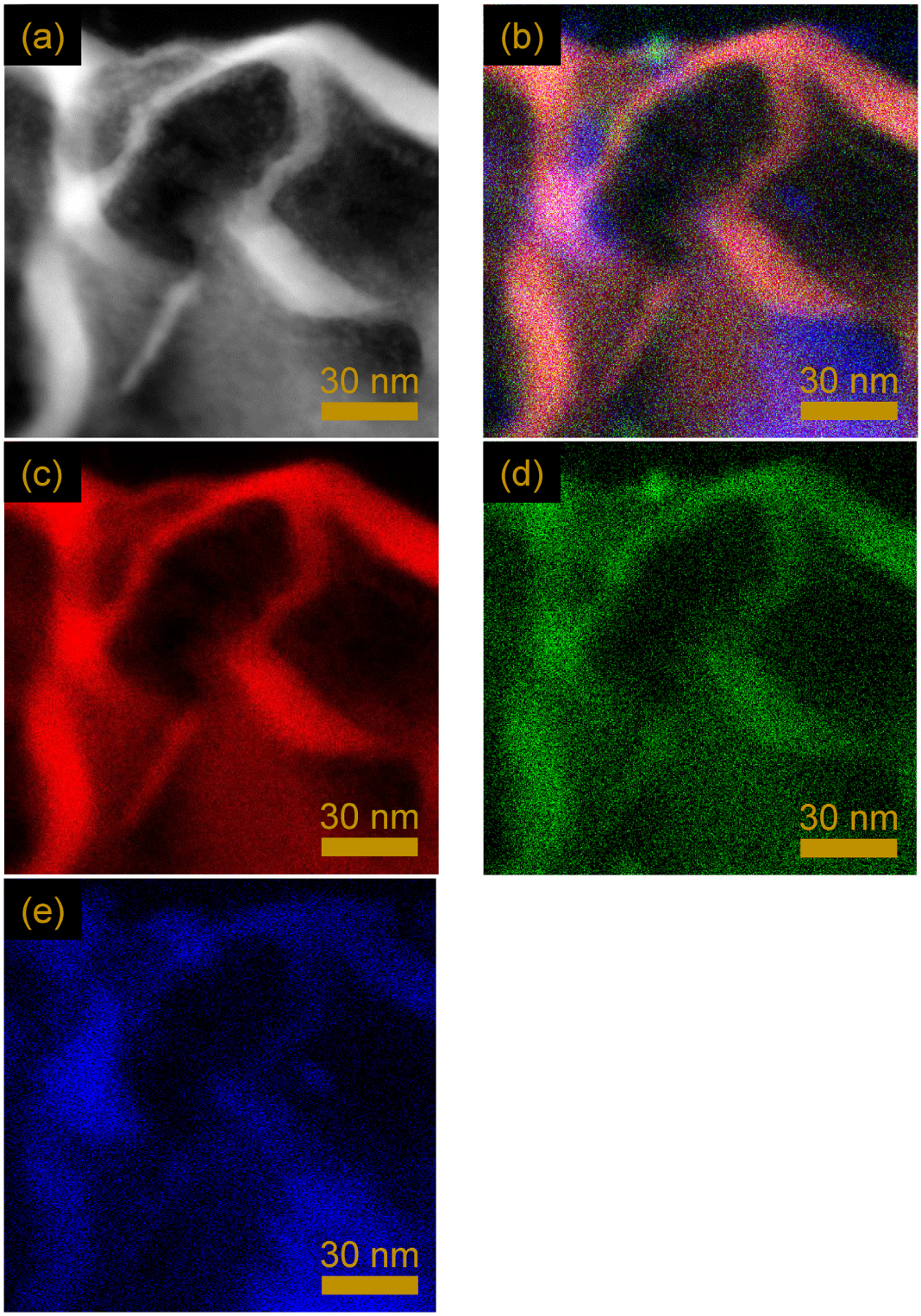

Fig. 9 – (a) STEM image and corresponding EDS elemental maps of (b) Ir + Ru + Ti, (c) Ir (red), (d) Ru (green), and (e) Ti (blue), for the Ir-1000/Ru-3000/Ti porous transport electrode after the 100-h durability test at 1.6 V.

200 mA cm^{-2} of the Ir-1000/Ru-3000/Ti, Ir-2000/Ru-2000/Ti, and Ir-3000/Ru-1000/Ti electrodes before and after the durability test at 1.6 V fixed for 100 h. The cell performance decreased after the 100-h durability test in all cases. The degradation was largest for the Ir-1000/Ru-3000/Ti electrode, followed by the Ir-2000/Ru-2000/Ti, the Ir-3000/Ru-1000/Ti, and the Ir-3000/Ti electrodes. Especially, Ir-1000/Ru-3000/Ti and Ir-2000/Ru-2000/Ti electrodes, with higher Ru ratios,

Please cite this article as: Yasutake M et al., Ru-core Ir-shell electrocatalysts deposited on a surface-modified Ti-based porous transport layer for polymer electrolyte membrane water electrolysis, International Journal of Hydrogen Energy, https://doi.org/10.1016/j.ijhydene.2023.07.048

Table 2 – The atomic ratio of Ir to Ru and Ti in each electrode. These ratios were obtained from the fibrous nanostructures consisting of Ir-shell layer, Ru-core layer, and Ti-oxide nanofiber, schematically described in the right bottom sub-figure of Fig. 1.

	Ir-1000/Ru-3000/Ti	Ir-2000/Ru-2000/Ti	Ir-3000/Ru-1000/Ti
Ir/Ru ratio before the durability test	0.28	0.92	2.0
Ir/Ru ratio after the durability test	No Ru detected	No Ru detected	No Ru detected
Ir/Ti ratio before the durability test	3.18	4.62	6.62
Ir/Ti ratio after the durability test	17.76	5.89	42.41

exhibited a greater degree of cell degradation. All overvoltages increased after the durability test, but especially the activation and mass transport overvoltages, as shown in Fig. 8b to d. In particular, the use of the Ir-1000/Ru-3000/Ti and Ir-2000/Ru-2000/Ti electrodes caused a significant increase in activation and mass transport overvoltages. In contrast, the mass transport overvoltage remains low in using the Ir-3000/Ru-1000/Ti electrode, even after the durability test.

Fig. 9 shows (a) a STEM image and (b-e) corresponding EDS elemental intensity maps of the Ir-1000/Ru-3000/Ti electrode after the 100-h durability test. Table 2 shows the atomic ratio of Ir to Ru (Ir/Ru) and the ratio of Ir to Ti (Ir/Ti) before and after the durability test, as analyzed by EDS. After the durability test, the Ir/Ru ratio of the Ir-1000/Ru-3000/Ti electrode increased significantly from 0.28 due to Ru dissolution. The Ir/Ru ratio of the other electrodes also increased by losing Ru. This means that the observed protection of Ru by the Ir coating was effective only within a short term, with the Ru-core dissolving in the long-term durability test. Therefore, optimizing the relative amounts of Ir and Ru loading and their ratios will be a critical matter in future studies in terms of improving the long-term durability.

Fig. 9 shows that the catalyst nanostructure changed significantly after the durability test. Table 2 quantitatively confirms a significant increase in the Ir to Ti (Ir/Ti) ratio, indicating a certain dissolution of the nanostructured TiO_2 fibers, leading to Ir detachment and therefore a decrease in the availability of Ir-based active sites. Such structural changes, including Ir detachment, increase the activation and mass transport overvoltages, especially for electrodes with a lower Ir ratio, as shown in Fig. 8c and d [42].

As shown in Table 2, both Ir and Ru coating may protect Ti dissolution, especially in the Ir-2000/Ru2000/Ti electrode. But the degradation may be caused mostly by Ru dissolution as the protective Ir coating on Ru was insufficient due to the low ratio of Ir to Ru. The ratio of Ir to Ru increased significantly in the Ir-2000/Ru-2000/Ti and Ir-3000/Ru-1000/Ti electrodes even with higher Ir ratios after the durability test, by Ru dissolution. Therefore, these results indicate a difficulty in maintaining long-term stability at 1.6 V, the dissolution potential of Ru, even in such a core-shell structure. Cell operation below 1.6 V may prevent such degradation associated with Ru dissolution. Although the Ir-3000/Ru-1000 electrode maintained its cell performance even after the durability test, the remaining Ir only could contribute to the OER reaction after the Ru dissolution. Thus, the core-shell catalysts with metallic iridium and ruthenium prepared in this study still have to improve their durability.

In order to improve the durability, alternative fabrication procedures should be considered to allow the Ir layer to fully cover the Ru layer. Selective deposition of the Ir layer on the Ru surface would be highly desired. In addition, the use of iridium oxide and ruthenium oxide rather than metallic Ir and Ru may improve their durability because these materials are more stable in such severe cell conditions [43]. Developing the RuO_2-core IrO_2-shell electrocatalyst deposited on the surface-modified PTL is therefore a prospective strategy for improving the stability of the core-shell structure. Much longer durability tests beyond 100 h, *e.g.*, at constant current/voltage will also be needed for practical applications of such PEMWE electrodes.

Performance at high current densities

Besides the reduction of PGM catalyst loading, high current density operation is also an effective way to reduce CAPEX. To evaluate the electrochemical performance of the core-shell catalyst decorated PTE in the high current density region, the I–V characteristics up to 12.5 A cm^{-2} were evaluated. The electrode used for the evaluation in the high current density range was the Ir-3000/Ru-1000/Ti electrode, which exhibited the highest electrochemical performance and durability and the lowest mass transport overvoltage compared to the other electrodes. In the test up to a high current density, the water supply flow rate was increased to 20 ml min^{-1}.

Fig. 10 shows the I–V characteristics of the cell with the Ir-3000/Ru-1000 electrode, confirming that no limiting current behavior was observed even at high current densities above

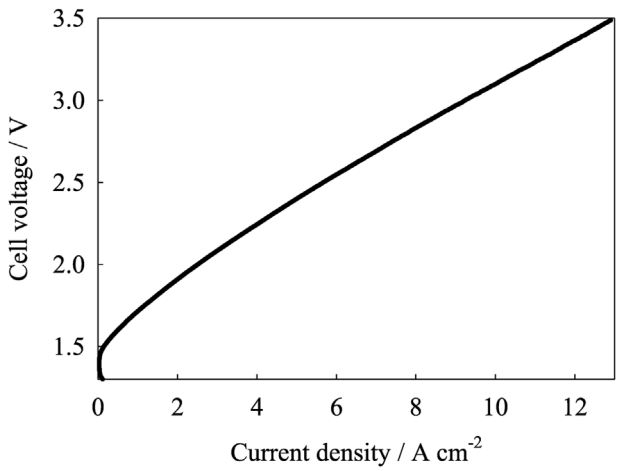

Fig. 10 – I–V characteristics of the PEMWE cell using the Ir-3000/Ru-1000/Ti PTE in the high current density region up to 12 A cm^{-2}.

Please cite this article as: Yasutake M et al., Ru-core Ir-shell electrocatalysts deposited on a surface-modified Ti-based porous transport layer for polymer electrolyte membrane water electrolysis, International Journal of Hydrogen Energy, https://doi.org/10.1016/j.ijhydene.2023.07.048

12 A cm^{-2}, and that electrolysis was stable even at high voltages above 3.5 V. It is however desirable to operate at a high current density below an electrolysis voltage of 2.0 V to prevent IrO_2 dissolution and below 1.6 V to prevent Ru dissolution. In this study, the electrolysis voltage in the high current density region is still significantly high due to the high ohmic overvoltage resulting from the use of a thicker electrolyte membrane, Nafion 117 (178 μm thick). The use of a thinner electrolyte membrane can reduce the electrolysis voltage in the high current density region. As the I–V characteristics did not show a significant increase in electrolysis voltage even at high current densities, this PTE structure could be effective for high current density operations leading to a reduction of the CAPEX of PEM electrolyzers, by reducing the overall electrode area.

Conclusions

Catalyst-integrated PTEs using Ru-core Ir-shell catalysts were directly deposited on the PTLs. The core-shell catalyst-integrated PTE exhibited higher electrolysis performance and lower activation overvoltage compared to conventional PTEs with the same iridium loading, indicating the possibility of reducing the amount of iridium used in PEM water electrolysis. Although the Ir-shell initially acted as a protective layer, the dissolution of Ru and Ti resulted in performance degradation during long-term durability tests, showing that an effective coating of Ir layer on Ru core remains as an important technical issue.

This highly porous electrode structure did not show a limiting current density even at 12 A cm^{-2}. Therefore, this unique highly porous electrode can significantly increase the current density of PEM water electrolysis. The total amount of PGM used on a conventional anode is 2–10 mg cm^{-2}, but the total PGM loading in the novel anode reported here was dramatically reduced to just 0.2 mg cm^{-2}, since no Pt coating is used. Therefore, the combination of (i) using a Ru-core Ir-shell structure to reduce the Ir loading (via a reduction in the activation overvoltage) and (ii) using a highly-porous catalyst-integrated PTE structure for reducing the overall electrode area (enabling high current density operation) has a potential to significantly reduce the CAPEX in PEM water electrolysis.

Declaration of competing interest

The authors declare that they have no known competing financial interests or personal relationships that could have appeared to influence the work reported in this paper.

Acknowledgments

Financial support from the Center of Innovation (COI) Program Grant Number JPMJCE1318 by the Japan Science and Technology Agency, Japan is gratefully acknowledged. A partial financial support by the Fukuoka Strategy Conference for Hydrogen Energy is also acknowledged.

REFERENCES

[1] Intergovernmental Panel on Climate Change. Technical summary. 2021. https://www.ipcc.ch/report/ar6/wg1/chapter/technical-summary/tergovernmental.
[2] Giuliano G, Stefano M, Yann M, Javier, Pose R, Ilja R, Bennett S, Johnstone N, Luis M. Innovation in batteries and electricity storage. 2020. https://www.actu-environnement.com/media/pdf/news-36144-etude-oeb-batteries-brevets.pdf.
[3] Hydrogen Council. Scaling up. November 2017. https://hydrogencouncil.com/wp-content/uploads/2017/11/Hydrogen-scaling-up-Hydrogen-Council.pdf.
[4] International Energy Agency. The future of hydrogen. 2019. https://www.iea.org/hydrogen2019/.
[5] Villagra A, Millet P. An analysis of PEM water electrolysis cells operating at elevated current densities. Int J Hydrogen Energy 2019;44:9708–17. https://doi.org/10.1016/j.ijhydene.2018.11.179.
[6] International Renewable Energy Agency. Green hydrogen cost reduction. 2020. https://www.irena.org/-/media/Files/IRENA/Agency/Publication/2020/Dec/IRENA_Green_hydrogen_cost_2020.pdf.
[7] Bizzotto F, Quinson J, Zana A, Kirkensgaard JJK, Dworzak A, Oezaslan M, Arenz M. Ir nanoparticles with ultrahigh dispersion as oxygen evolution reaction (OER) catalysts: synthesis and activity benchmarking. Catal Sci Technol 2019;9:6345–56. https://doi.org/10.1039/c9cy01728c.
[8] Baik C, Lee SW, Pak C. Glycine-induced ultrahigh-surface-area IrO2@IrOx catalyst with balanced activity and stability for efficient water splitting. Electrochim Acta 2021;390:138885. https://doi.org/10.1016/j.electacta.2021.138885.
[9] Park JE, Kim S, Kim OH, Ahn CY, Kim MJ, Kang SY, Jeon TI, Shim JG, Lee DW, Lee JH, Cho YH, Sung YE. Ultra-low loading of IrO_2 with an inverse-opal structure in a polymer-exchange membrane water electrolysis. Nano Energy 2019;58:158–66. https://doi.org/10.1016/j.nanoen.2019.01.043.
[10] Chatterjee S, Peng X, Intikhab S, Zeng G, Kariuki NN, Myers DJ, Danilovic N, Snyder J. Nanoporous iridium nanosheets for polymer electrolyte membrane electrolysis. Adv Energy Mater 2021;11:1–11. https://doi.org/10.1002/aenm.202101438.
[11] Nong HN, Gan L, Willinger E, Teschner D, Strasser P. IrOx core-shell nanocatalysts for cost- and energy-efficient electrochemical water splitting. Chem Sci 2014;5:2955–63. https://doi.org/10.1039/c4sc01065e.
[12] Nong HN, Oh HS, Reier T, Willinger E, Willinger MG, Petkov V, Teschner D, Strasser P. Oxide-supported $IrNiO_x$ core-shell particles as efficient, cost-effective, and stable catalysts for electrochemical water splitting. Angew Chem Int Ed 2015;54:2975–9. https://doi.org/10.1002/anie.201411072.
[13] Yeo RS, Orehotsky J, Visscher W, Srinivasan S. Ruthenium-based mixed oxides as electrocatalysts for oxygen evolution in acid electrolytes. J Electrochem Soc 1981;128:1900–4. https://doi.org/10.1149/1.2127761.
[14] Cheng J, Zhang H, Chen G, Zhang Y. Study of $Ir_xRu_{1-x}O_2$ oxides as anodic electrocatalysts for solid polymer electrolyte water electrolysis. Electrochim Acta 2009;54:6250–6. https://doi.org/10.1016/j.electacta.2009.05.090.
[15] Wen Y, Chen P, Wang L, Li S, Wang Z, Abed J, Mao X, Min Y, Dinh CT, Luna PD, Huang R, Zhang L, Wang L, Wang L, Nielsen RJ, Zhuang HLT, Voznyy CKO, Li YHY, Goddard III WA, Zhang B, Peng H, Sargent EH. Stabilizing highly active Ru sites by suppressing lattice oxygen

Please cite this article as: Yasutake M et al., Ru-core Ir-shell electrocatalysts deposited on a surface-modified Ti-based porous transport layer for polymer electrolyte membrane water electrolysis, International Journal of Hydrogen Energy, https://doi.org/10.1016/j.ijhydene.2023.07.048

participation in acidic water oxidation. J Am Chem Soc 2021;143:6482–90. https://doi.org/10.1021/jacs.1c00384.

[16] Kwon T, Yu A, Kim S jin, Kim MH, Lee C, Lee Y. Au-Ru alloy nanofibers as a highly stable and active bifunctional electrocatalyst for acidic water splitting. Appl Surf Sci 2021;563:150293. https://doi.org/10.1016/j.apsusc.2021.150293.

[17] Trasatti S. Electrocatalysis in the anodic evolution of oxygen and chlorine. Electrochim Acta 1984;29:1503–12. https://doi.org/10.1016/0013-4686(84)85004-5.

[18] Doan TL, Lee HE, Shah SSH, Kim MJ, Kim CH, Cho HS, Kim T. A review of the porous transport layer in polymer electrolyte membrane water electrolysis. Int J Energy Res 2021;45:14207–20. https://doi.org/10.1002/er.6739.

[19] Li G, Yu H, Song W, Wang X, Li Y, Shao Z, Yi B. Zeolite-templated $Ir_xRu_{1-x}O_2$ electrocatalysts for oxygen evolution reaction in solid polymer electrolyte water electrolyzers. Int J Hydrogen Energy 2012;37:16786–94. https://doi.org/10.1016/j.ijhydene.2012.08.087.

[20] Saveleva VA, Wang L, Luo W, Zafeiratos S, Ulhaq-Bouillet C, Gago AS, Friedrich KA, Savinova ER. Uncovering the stabilization mechanism in bimetallic ruthenium-iridium anodes for proton exchange membrane electrolyzers. J Phys Chem Lett 2016;7:3240–5. https://doi.org/10.1021/acs.jpclett.6b01500.

[21] Boodts JFC, Trasatti S. Effect of composition on the electrocatalytic activity of the ternary oxide $Ru_{0.3}Ti_{(0.7-x)}Sn_xO_2$: I. Oxygen evolution from $HClO_4$ solutions. J Electrochem Soc 1990;137:3784–9. https://doi.org/10.1149/1.2086301.

[22] Neyerlin KC, Bugosh G, Forgie R, Liu Z, Strasser P. Combinatorial study of high-surface-area binary and ternary electrocatalysts for the oxygen evolution reaction. J Electrochem Soc 2009;156:B363. https://doi.org/10.1149/1.3049820.

[23] Forgie R, Bugosh G, Neyerlin KC, Liu Z, Strasser P. Bimetallic Ru electrocatalysts for the OER and electrolytic water splitting in acidic media. Electrochem Solid State Lett 2010;13:1–5. https://doi.org/10.1149/1.3290735.

[24] Wu D, Kusada K, Yoshioka S, Yamamoto T, Toriyama T, Matsumura S, Chen Y, Seo O, Kim J, Song C, Hiroi S, Sakata O, Ina T, Kawaguchi S, Kubota Y, Kobayashi H, Kitagawa H. Efficient overall water splitting in acid with anisotropic metal nanosheets. Nat Commun 2021;12:1–9. https://doi.org/10.1038/s41467-021-20956-4.

[25] Audichon T, Napporn TW, Canaff C, Morais C, Comminges C, Kokoh KB. IrO_2 coated on RuO_2 as efficient and stable electroactive nanocatalysts for electrochemical water splitting. J Phys Chem C 2016;120:2562–73. https://doi.org/10.1021/acs.jpcc.5b11868.

[26] Seow JZY, Nguyen TD. Electrochemically assisted synthesis of ultra-small Ru@IrOx core-shell nanoparticles for water splitting electro-catalysis. Electrochim Acta 2020;341:136058. https://doi.org/10.1016/j.electacta.2020.136058.

[27] Shan J, Guo C, Zhu Y, Chen S, Song L, Jaroniec M, Zheng Y, Qiao SZ. Charge-redistribution-enhanced nanocrystalline $Ru@IrO_x$ electrocatalysts for oxygen evolution in acidic media. Chem 2019;5:445–59. https://doi.org/10.1016/j.chempr.2018.11.010.

[28] Mo J, Kang Z, Retterer ST, Cullen DA, Toops TJ, Green JB, Mench MM, Zhang FY. Discovery of true electrochemical reactions for ultrahigh catalyst mass activity in water splitting. Sci Adv 2016;2. https://doi.org/10.1126/sciadv.1600690.

[29] Lee BS, Ahn SH, Park HY, Choi I, Yoo SJ, Kim HJ, Henkensmeier D, Kim JY, Park S, Nam SW, Lee KY, Jang JH. Development of electrodeposited IrO2 electrodes as anodes in polymer electrolyte membrane water electrolysis. Appl Catal B Environ 2015;179:285–91. https://doi.org/10.1016/j.apcatb.2015.05.027.

[30] Kim H, Kim J, Kim J, Han GH, Guo W, Hong S, Park HS, Jang HW, Kim SY, Ahn SH. Dendritic gold-supported iridium/iridium oxide ultra-low loading electrodes for high-performance proton exchange membrane water electrolyzer. Appl Catal B Environ 2021;283:119596. https://doi.org/10.1016/j.apcatb.2020.119596.

[31] Laube A, Hofer A, Ressel S, Chica A, Bachmann J, Struckmann T. PEM water electrolysis cells with catalyst coating by atomic layer deposition. Int J Hydrogen Energy 2021;46:38972–82. https://doi.org/10.1016/j.ijhydene.2021.09.153.

[32] Kawachino D, Yasutake M, Odoi H, Noda Z, Matsuda J, Hayashi A, Sasaki K. Carbon-free all-in-one electrode using porous Ti sheet for PEFCs. ECS Trans 2018;86:541–7. https://doi.org/10.1149/08613.0541ecst.

[33] Yasutake M, Kawachino D, Noda Z, Matsuda J, Ito K, Hayashi A, Sasaki K. GDL-integrated electrodes with Ir-based electrocatalysts for polymer electrolyte membrane water electrolysis. ECS Trans 2019;92:833–43. https://doi.org/10.1149/09208.0833ecst.

[34] Kawachino D, Yasutake M, Noda Z, Matsuda J, Lyth SM, Hayashi A, Sasaki K. Surface-modified titanium fibers as durable carbon-free platinum catalyst supports for polymer electrolyte fuel cells. J Electrochem Soc 2020;167:104513. https://doi.org/10.1149/1945-7111/ab9cd4.

[35] Yasutake M, Anai H, Kawachino D, Noda Z, Matsuda J, Ito K, Hayashi A, Sasaki K. Metal-oxide-supported Ir-decorated electrocatalysts for polymer electrolyte membrane water electrolysis. ECS Trans 2018;86:673–82. https://doi.org/10.1149/08613.0673ecst.

[36] Yasutake M, Kawachino D, Noda Z, Matsuda J, Lyth SM, Ito K, Hayashi A, Sasaki K. Catalyst-integrated gas diffusion electrodes for polymer electrolyte membrane water electrolysis: porous titanium sheets with nanostructured TiO_2 surfaces decorated with Ir electrocatalysts. J Electrochem Soc 2020;167:124523. https://doi.org/10.1149/1945-7111/abb37d.

[37] Agawa Y, Kunimatsu M, Ito T, Kuwahara Y, Yamashita H. Preparation of Pt/C catalyst by coaxial arc plasma deposition for polymer electrolyte membrane fuel cells. ECS Electrochem Lett 2015;4:F57–60. https://doi.org/10.1149/2.0091510eel.

[38] Okumura M, Noda Z, Matsuda J, Tachikawa Y, Nishihara M, Lyth SM, Hayashi A, Sasaki K. Correlating cathode microstructure with PEFC performance using FIB-SEM and TEM. J Electrochem Soc 2017;164:F928–34. https://doi.org/10.1149/2.0581709jes.

[39] Lewinski KA, van der Vliet D, Luopa SM. NSTF advances for PEM electrolysis - the effect of alloying on activity of NSTF electrolyzer catalysts and performance of NSTF based PEM electrolyzers. ECS Trans 2015;69:893–917. https://doi.org/10.1149/06917.0893ecst.

[40] Xu C, Yang J, Liu E, Jia Q, Veith GM, Nair G, DiPietro S, Sun K, Chen J, Pietrasz P, Lu Zijie, Janger M, Gath KK, Mukerjee S, Waldecker JR. Physical vapor deposition process for engineering Pt based oxygen reduction reaction catalysts on NbOx templated carbon support. J Power Sources 2020;451:227709. https://doi.org/10.1016/j.jpowsour.2020.227709.

[41] Reier T, Oezaslan M, Strasser P. Electrocatalytic oxygen evolution reaction (OER) on Ru, Ir, and Pt catalysts: a comparative study of nanoparticles and bulk materials. ACS Catal 2012;2:1765–72. https://doi.org/10.1021/cs3003098.

[42] Taie Z, Peng X, Kulkarni D, Zenyuk IV, Weber AZ, Hagen C, Danilovic N. Pathway to Complete energy sector decarbonization with available iridium resources using

Please cite this article as: Yasutake M et al., Ru-core Ir-shell electrocatalysts deposited on a surface-modified Ti-based porous transport layer for polymer electrolyte membrane water electrolysis, International Journal of Hydrogen Energy, https://doi.org/10.1016/j.ijhydene.2023.07.048

ultralow loaded water electrolyzers. ACS Appl Mater Interfaces 2020;12:52701–12. https://doi.org/10.1021/acsami.0c15687.

[43] Cherevko S, Geiger S, Kasian O, Kulyk N, Grote J, Savan A, Shrestha BR, Merzlikin S, Breitbach B, Ludwig A, Mayrhofer KJJ. Oxygen and hydrogen evolution reactions on Ru, RuO_2, Ir, and IrO_2 thin film electrodes in acidic and alkaline electrolytes : a comparative study on activity and stability. Catal Today 2016;262:170–8. https://doi.org/10.1016/j.cattod.2015.08.014.

Please cite this article as: Yasutake M et al., Ru-core Ir-shell electrocatalysts deposited on a surface-modified Ti-based porous transport layer for polymer electrolyte membrane water electrolysis, International Journal of Hydrogen Energy, https://doi.org/10.1016/j.ijhydene.2023.07.048